Electronic Supplementary Information

Low thermal quenching of metal halide based metal–organic framework phosphor for light-emitting diodes

Xiao-Gang Yang,* Ying-Jun Chen, Pei-Pei Yin, Yan Li, Shu-Yao Yang, Yi-Man Li, and Lu-Fang Ma*

College of Chemistry and Chemical Engineering, Luoyang Normal University, Henan Key Laboratory of Function-Oriented Porous Materials, Luoyang 471934, P. R. China.

Corresponding Author

*E-mail: yxg2233@126.com; mazhuxp@126.com

1. Experimental Section

1.1. Materials and methods

All the starting reagents and solvents were commercially available and used as received without further purification. Powder X-ray diffraction (PXRD) patterns were measured at room temperature using a Bruker D8-ADVANCE X-ray diffractometer with Cu *Kα* radiation (λ = 1.5418 Å). Intensity data were collected in a 2θ range of 5-50° with a step of 0.02° (2*θ*) and a counting time of 0.2 s/step. Elemental analyses for C, H, and N were carried out on a Flash 2000 organic elemental analyzer. The IR spectrum was recorded in the range of 4000–400 cm^{-1} on a Nicolet 6700 (Thermo) FT-IR spectrometer with KBr pellets. Thermalgravimetric analyses (TGA) was carried out on a SDT Q600 thermogravimetric analyzer with a heating rate of 10 °C/min under a N_2 atmosphere. Photoluminescence (PL) spectra and decay curve were tested on Edinburgh FLS1000 fluorescence spectrometer equipped with a xenon arc lamp (Xe900) for fluorescence spectra, nanosecond flash-lamp (nF900) for PL decay curve. The temperature dependence PL spectra were measured using a temperature controller attached to a cryostat (Oxford Ltd. Optistat DN2) using an FLS1000 fluorescence spectrometer.

1.2. Synthesis of [$CdCl_2$(AD)]

A mixture of acridine (0.2 mmol, 35.844 mg), $CdCl_2$ (0.2 mmol, 45.672 mg), and EtOH (8 mL) was sealed in a 25 mL Teflon-lined stainless steel vessel reactor. The mixture was heated at 120 ºC for 3 hours, and then cooled to room temperature about 8 hours. Light-yellow crystals of [$CdCl_2$(AD)] were obtained. Then, washed with

ethanol several times and filtered, dried in natural environment. Elemental analysis calcd. (%) for $C_{13}H_9CdCl_2N$: C 43.06, H 2.50, N 3.86; found (%): C 43.26, H 2.11, N 3.34. FT-IR (cm^{-1}): 3052 w, 1620 s, 1563 s, 1518 s, 1465 s, 1390 m, 1293 m, 966 s, 930 s, 784 s, 731 s, 664 s, 479 m.

1.3. X-ray crystal structure

Single-crystal X-ray diffraction data for [$CdCl_2$(AD)] was obtained at room temperature (293K) on an Oxford Diffraction SuperNova area-detector diffractometer using mirror optics monochromated Mo Kα radiation (λ = 0.71073 Å). The Data collection, data reduction and empirical absorption correction were performed by CrysAlisPro.[1] The crystal structure were solved by direct methods, using SHELXS-2014[2] and least-squares refined with SHELXL-2014[3] using anisotropic thermal displacement parameters for all non-hydrogen atoms. The crystallographic data and selected bond lengths and angles for [$CdCl_2$(AD)] were listed in Tables S1 and S2. The CIF file of [$CdCl_2$(AD)] (CCDC No. 2364270) can be acquired free of charge from the Cambridge Crystallographic Date Centre via http://www.ccdc.cam.ac.uk/conts/retrieving.html.

1.4. Electronic structure calculations

The density functional theory (DFT) and charge density distribution were carried out using Dmol3[4] and CASTEP[5] module in Material Studio software package,[6] respectively. All calculations were performed based on the crystallographic information file (cif) from the single-crystal structure of [$CdCl_2$(AD)]. The initial geometrical optimizations of the ground state was carried out by Perdew-Wang

(PW91) generalized gradient approximation (GGA) method with the double numerical basis sets plus polarization function (DNP). The self-consistent field (SCF) converged criterion was within 1.0×10^{-5} hartree $atom^{-1}$ and the converging criterion of the structure optimization was 1.0×10^{-3} hartree $bohr^{-1}$. The Brillouin zone is sampled by 1 × 1 × 1 k-points, and test calculations reveal that the increase of k-points does not affect the results.

1.5. Photocatalytic degradation of dye

The photocatalytic activities of the **1** were evaluated by the degradation of methyl orange (MO) under 300 W xenon lamp illumination. A certain amount of photocatalyst **1** (10 mg) was immersed in 30 mL MO (20 mg/L) aqueous solution for reserve. Before irradiation, the suspension was magnetically stirred in the dark for 30 min to achieve the adsorption-desorption equilibrium. Then the mixture solution was exposed to light source, the suspension was centrifuged and then detected by ultraviolet-visible spectrophotometer analysis with a interval of 20 min. Changes in the maximum absorbance of 464 nm was measured spectrophotometrically to determine the decrease in the concentration of the MO.

1.6. Optoelectronic measurements.

Photoelectronic behaviors of **1** were tested by Chenhua CHI 660E electrochemical workstation in a standard three-electrode system with 0.5 M sodium sulfate aqueous solution as electrolyte, platinum wire as counter electrode, Ag/AgCl as the reference electrode, and powder of **1** coated on indium tin oxide (ITO) as working electrode (1.0 cm^2). It was conducted in a quartz glass reactor of ca. 50 cm^3 and irradiated by a

300 W xenon lamp. The electrochemical impedance spectroscopy Nyquist plots were recorded at 0 V potential in the frequency range of 100 kHz to 100 MHz, and transient photocurrent responses with the on-off cycle's illumination were tested in the three-electrode system at ambient pressure and room temperature.

1.7. Fabrication of LED devices

1.7.1. Fabrication of green LED device

40 mg [$CdCl_2$(AD)] phosphor was thoroughly mixed with about 20 mL epoxy resin. The mixture was coated on a 365 nm diode chip, and then and then heated at 100 ºC for 1 hour.

1.7.2. Fabrication of white LED device

30 mg [$CdCl_2$(AD)] phosphor and 10 mg commercial N630 red phosphor was thoroughly mixed with about 20 mL epoxy resin. The mixture was coated on a 460 nm diode chip, and then and then heated at 100 ºC for 1 hour.

2. Supporting Figures

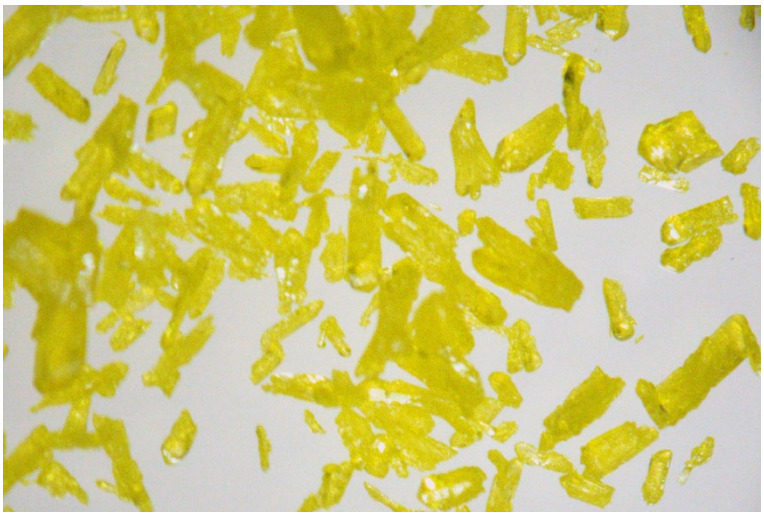

Figure S1. Digital photograph of the crystals of title complex **1** synthesized under solvothermal condition.

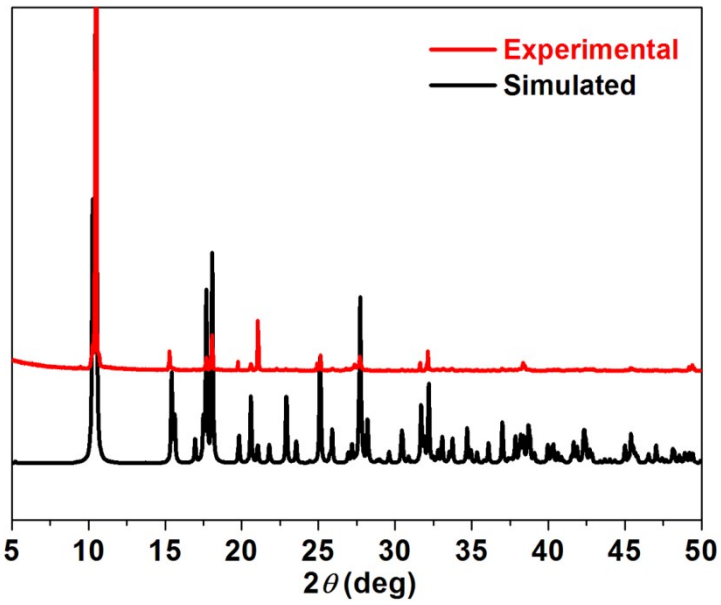

Figure S2. Powder X-ray diffraction (PXRD) patterns of simulated (black) and as-prepared (red) [$CdCl_2$(AD)] (**1**) obtained under solvothermal condition.

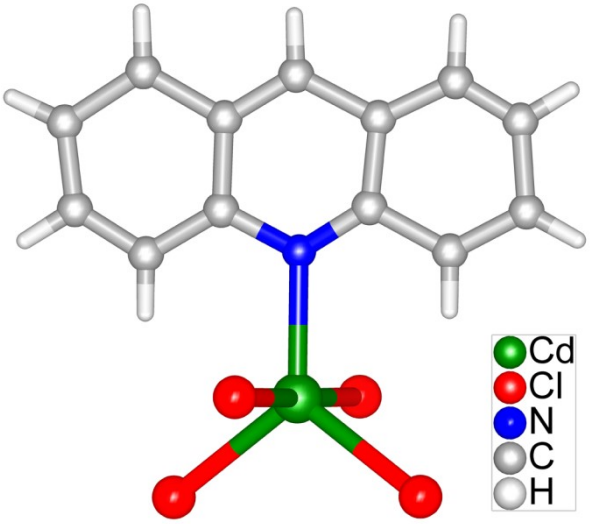

Figure S3. View of local coordination environment of Cd(II) atom in **1**.

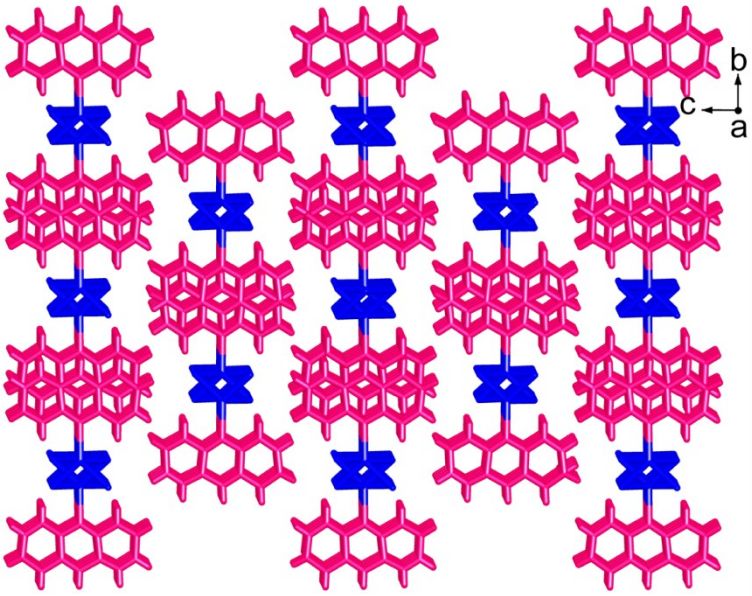

Figure S4. View of the 3D structure of **1** showing an alternating arrangement of $CdCl_2$ inorganic chains electronic acceptor (blue) and AD π-conjugated system electronic donor (rose red).

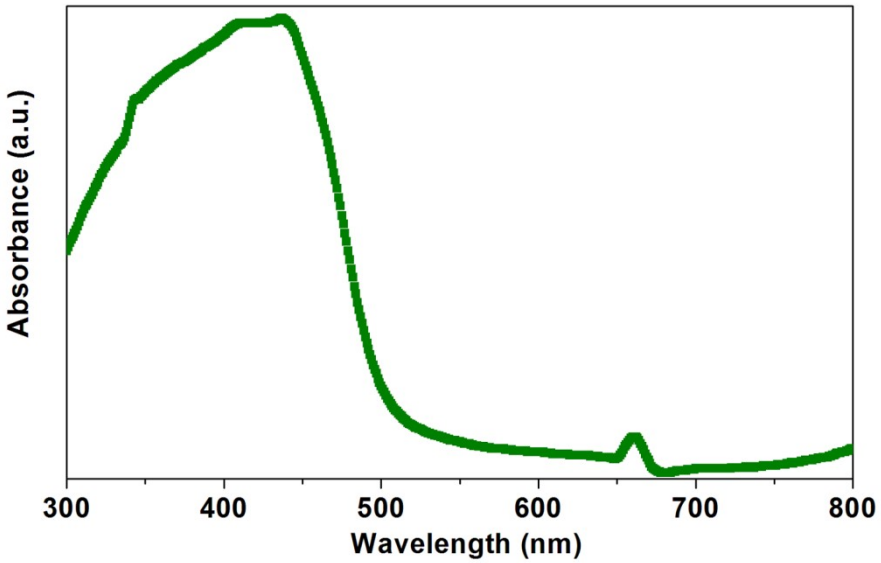

Figure S5. UV−vis absorption spectrum of **1** in solid state measured at room temperature.

Figure S6. Digital photograph of the as-prepared powder sample of **1** under UV (365 nm) light.

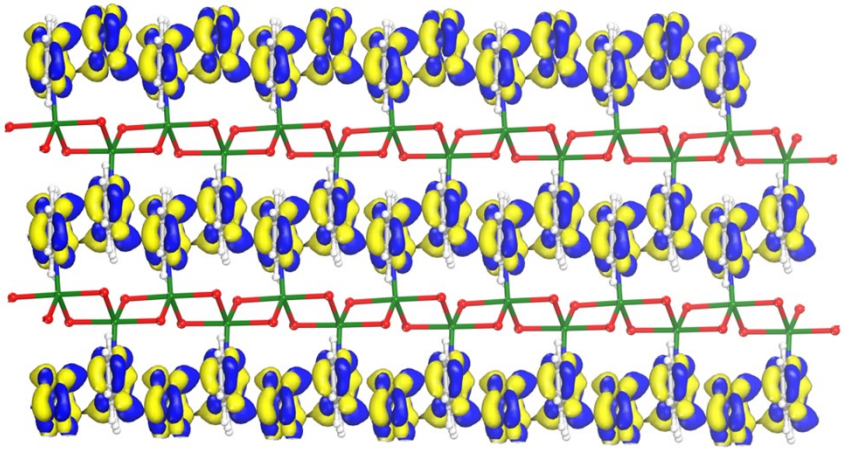

(a)

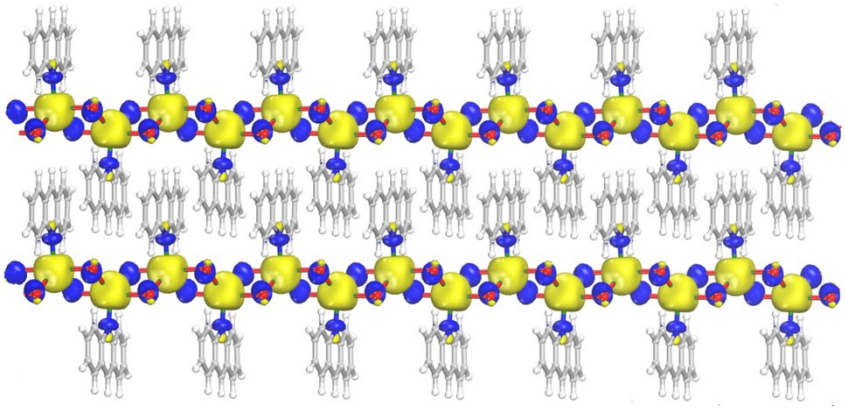

(b)

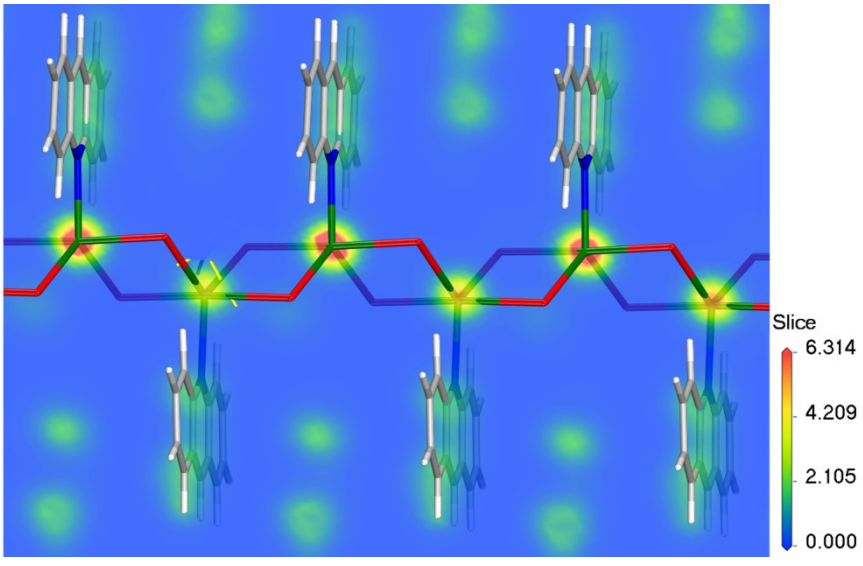

(c)

Figure S7. View of the HOMO (a) and LUMO (b) for the DFT optimized structure of **1**. (c) Calculated charge density distribution of **1**.

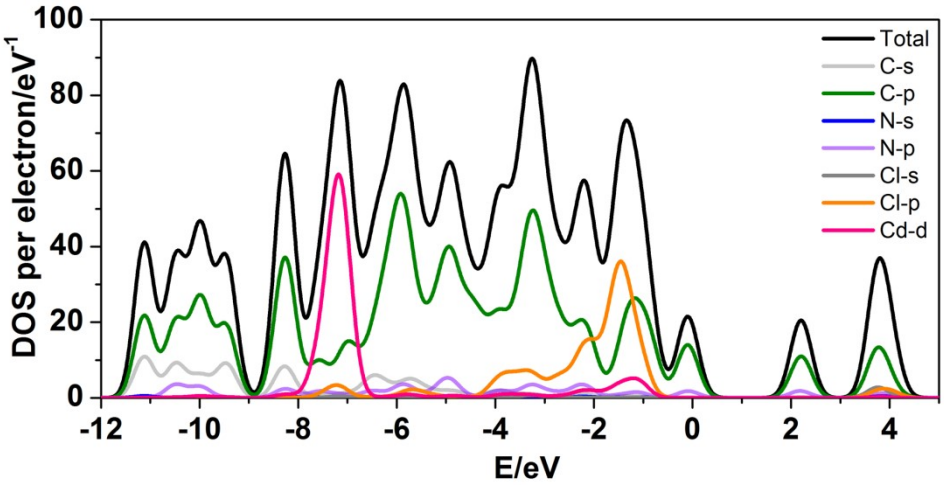

Figure S8. Partial electronic density of states (PDOS) of **1**.

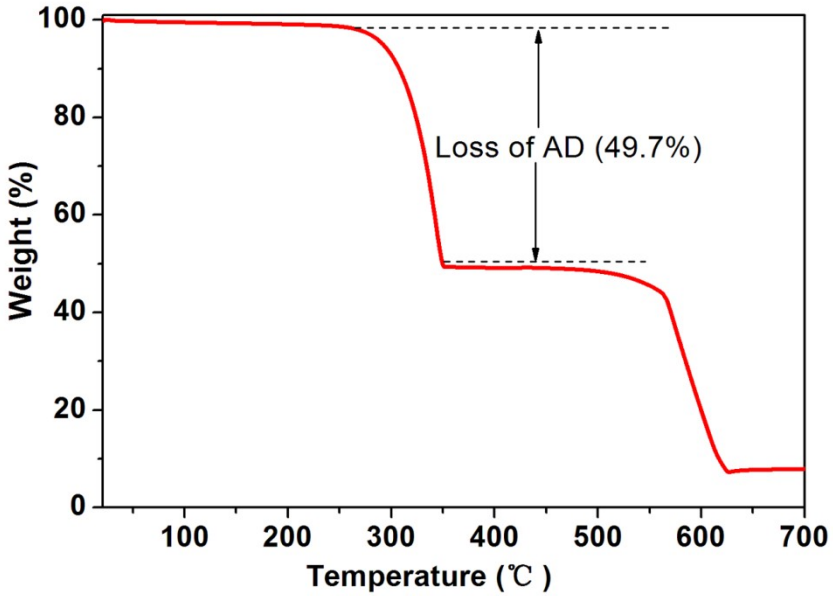

Figure S9. Thermogravimetric analysis curve of **1**.

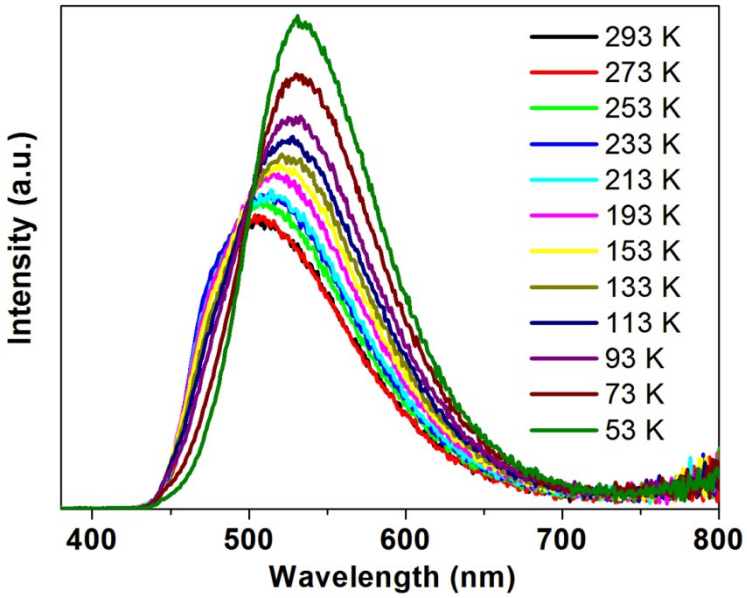

(a)

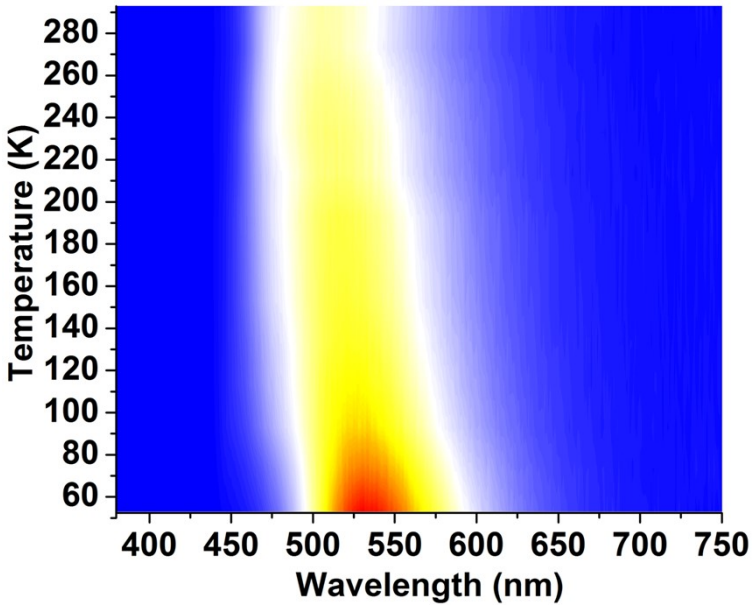

(b)

Figure S10. (a) Temperature-dependent PL spectra of **1** in the temperature range of 293–53 K excited at 360 nm. (b) Two-dimensional plot showing the PL spectra of **1** recorded in the temperature range of 293–53 K excited at 360 nm.

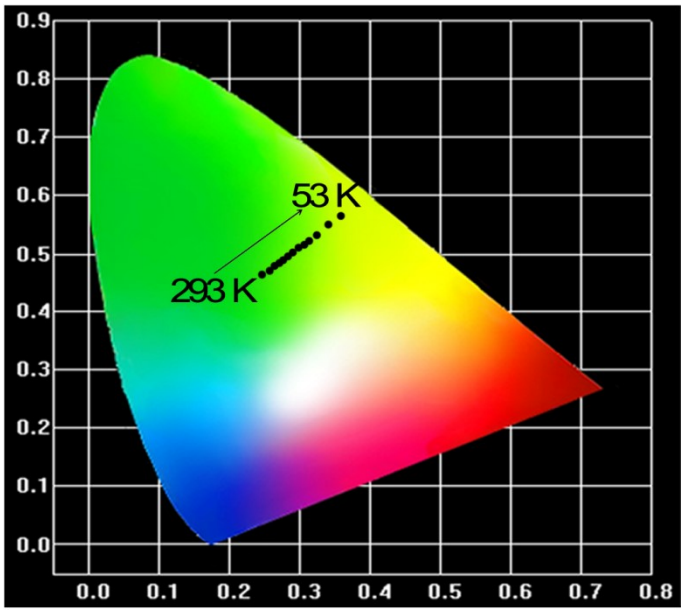

Figure S11. CIE-1931 chromaticity diagram showing emission of **1** from 293 to 53 K.

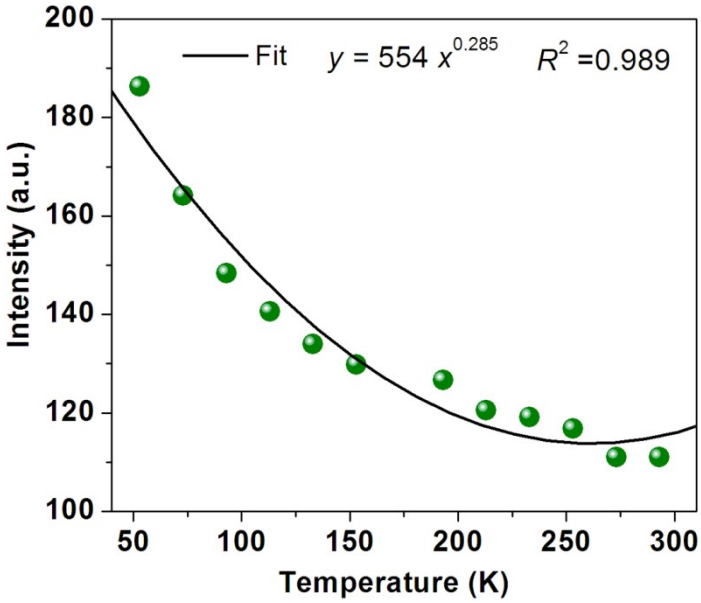

Figure S12. Temperature-dependent maximum PL intensity and the fitted curve in the temperature range of 53–293 K.

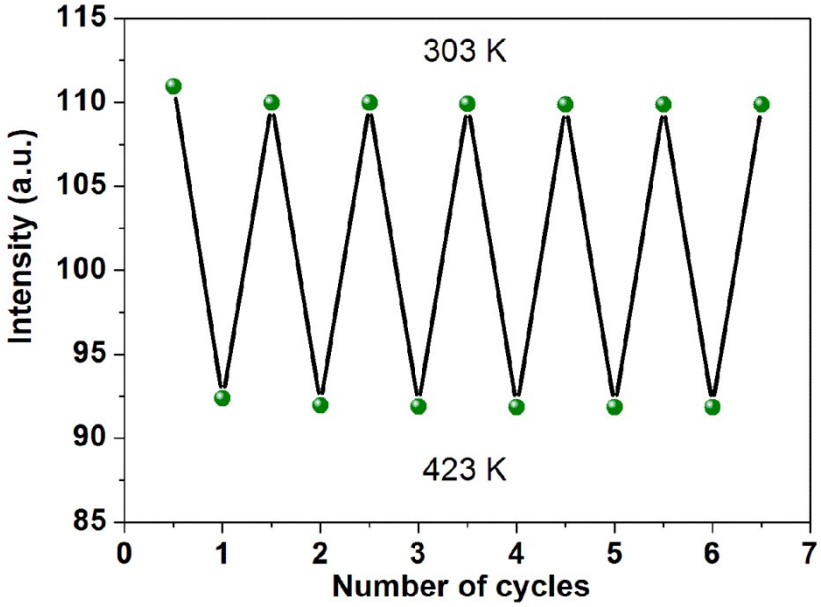

Figure S13. Reversible variation of the PL intensity of **1** between 303 and 423 K.

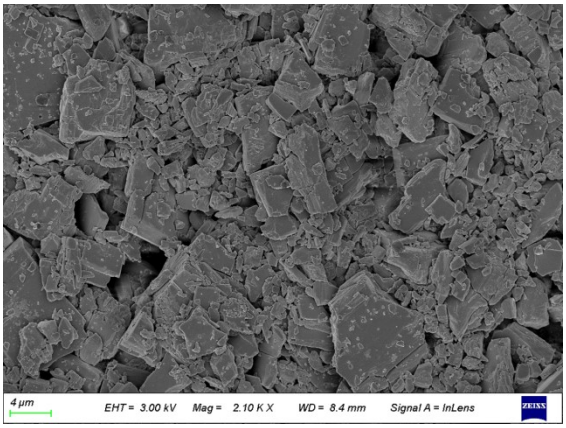

(a)

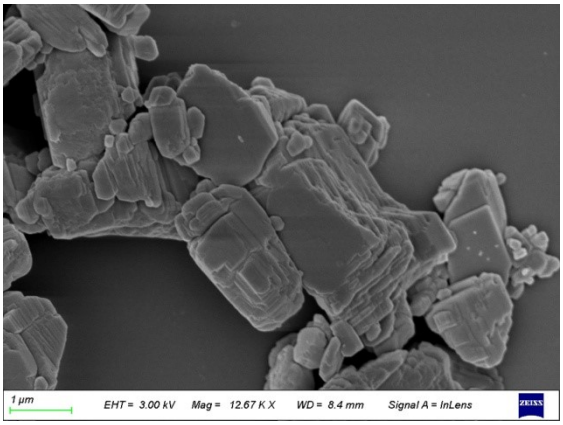

(b)

Figure S14. SEM images of **1** before (a) and after soaking in water for 60 days (b).

.

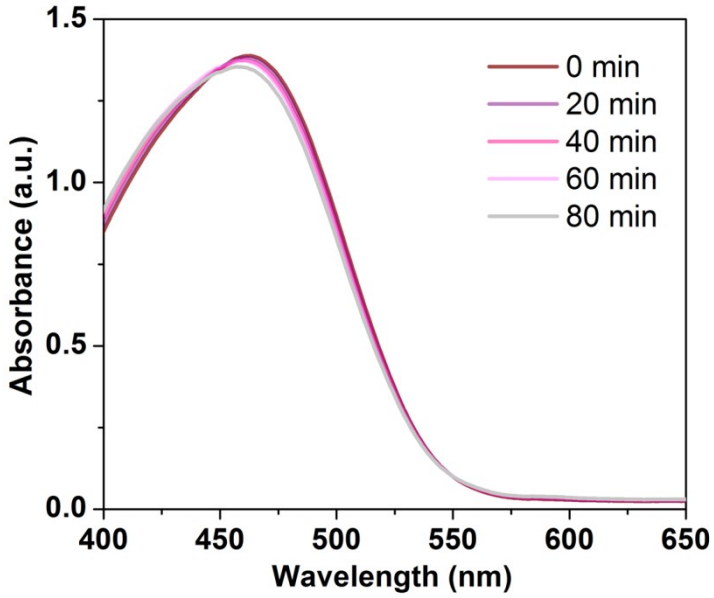

(a)

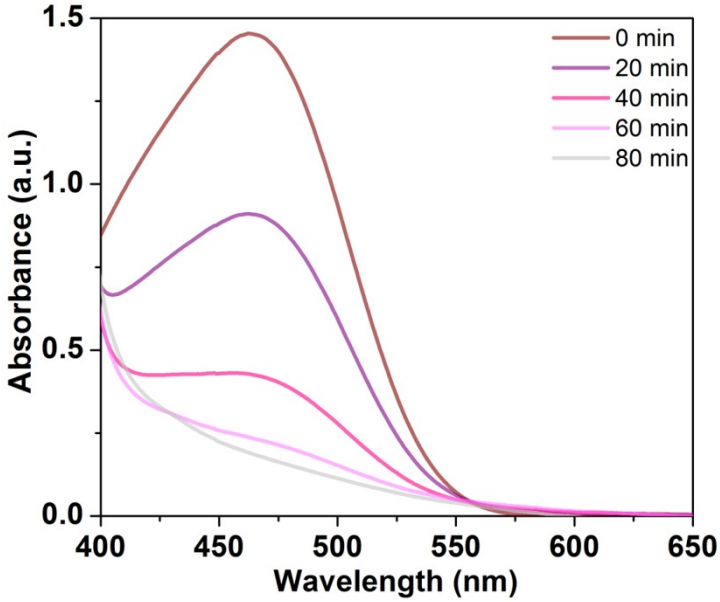

(b)

Figure S15. (a) Self-degradation of MO aqueous solution irradiated under light irradiation by detecting the maximum absorbance peak at 464 nm. (b) Degradation diagram of MO with presence of the powder of **1** (10 mg) under illumination.

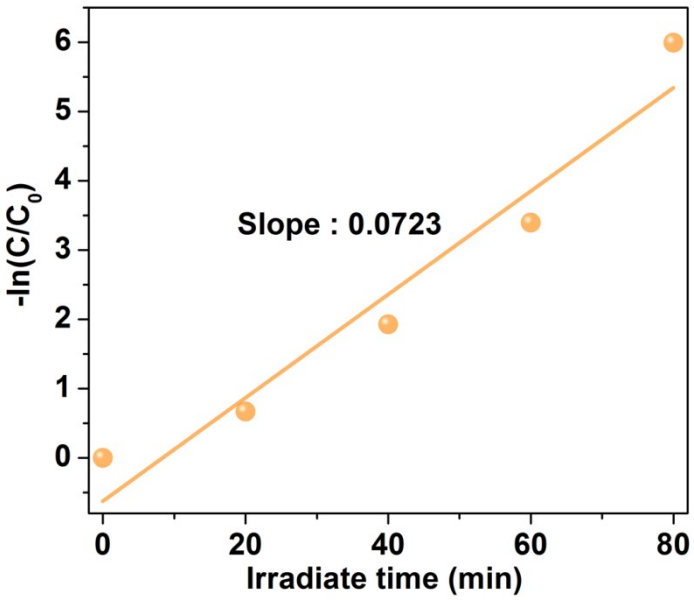

Figure S16. Rate constants of photocatalytic degradation for MO with presence of the powder of **1** (10 mg) under illumination.

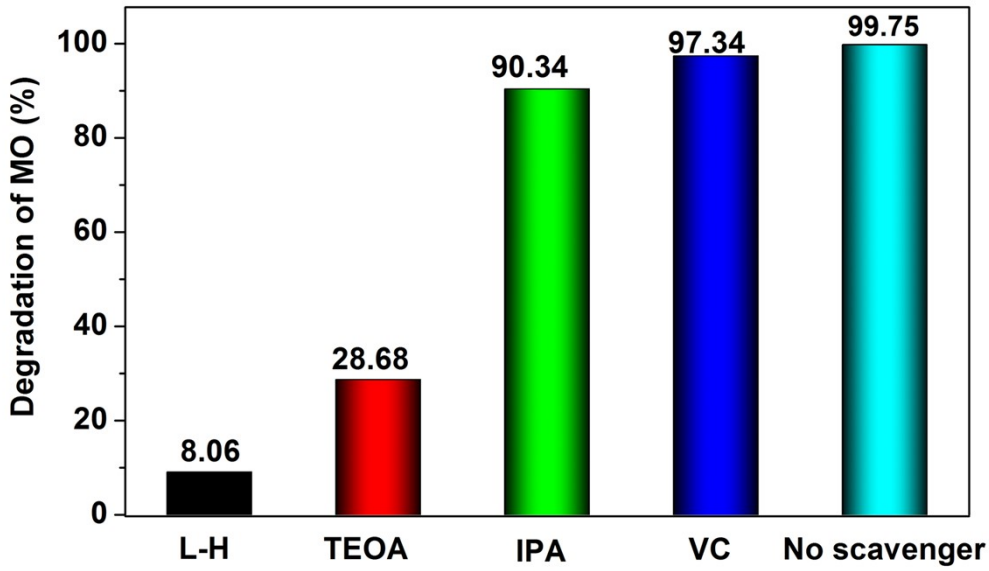

Figure S17. Bar chart of degradation rate for the detection of active species in the photocatalytic process of **1** by adding different scavengers. L-Histidine (L-H) for singlet oxygen ($^1O_2$), Triethanolamine (TEOA) for hole (h^+), propan-2-ol (IPA) for hydroxyl radicals (·OH), and Vitamin C (VC) for superoxide radicals ($\cdot O_2^-$).

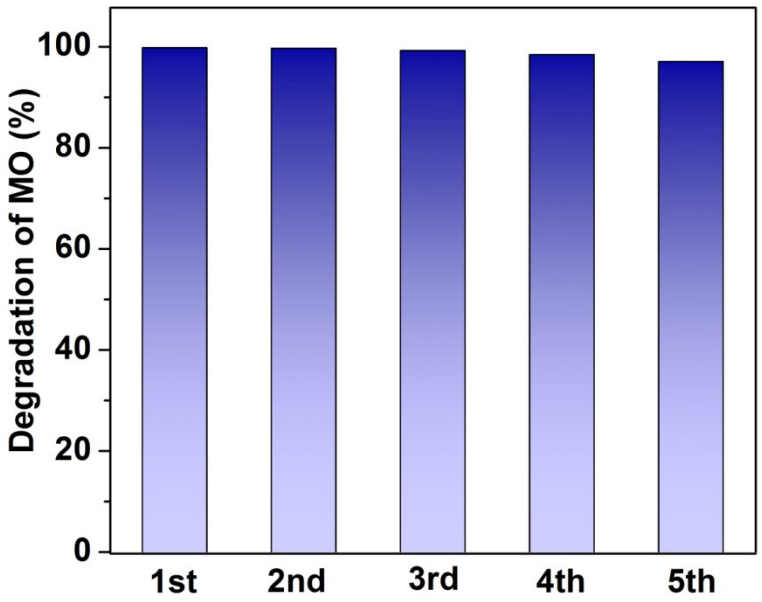

Figure S18. The reusability of **1** for the photocatalytic degradation of MO.

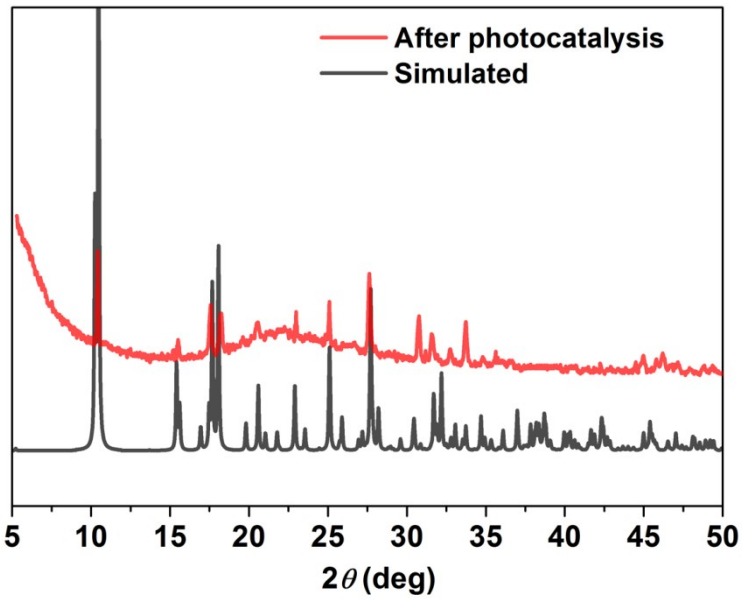

Figure S19. PXRD of **1** after photocatalytic degradation of MO.

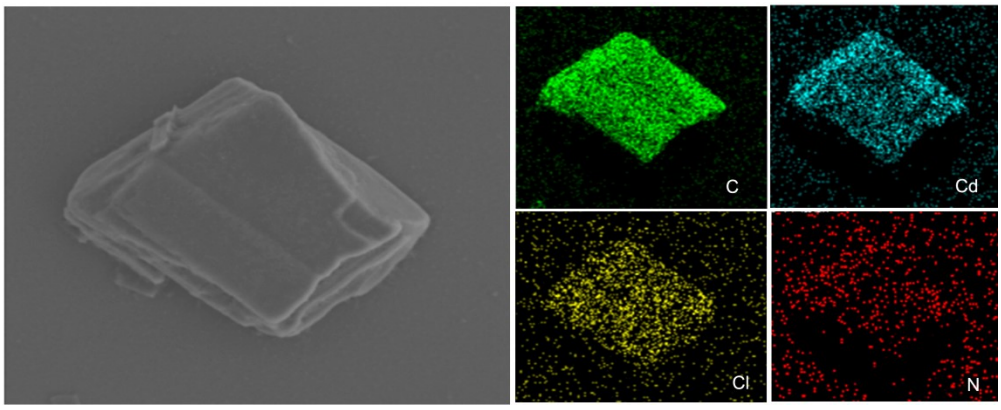

Figure S20. SEM image and elemental mapping images of **1** after photocatalytic degradation of MO.

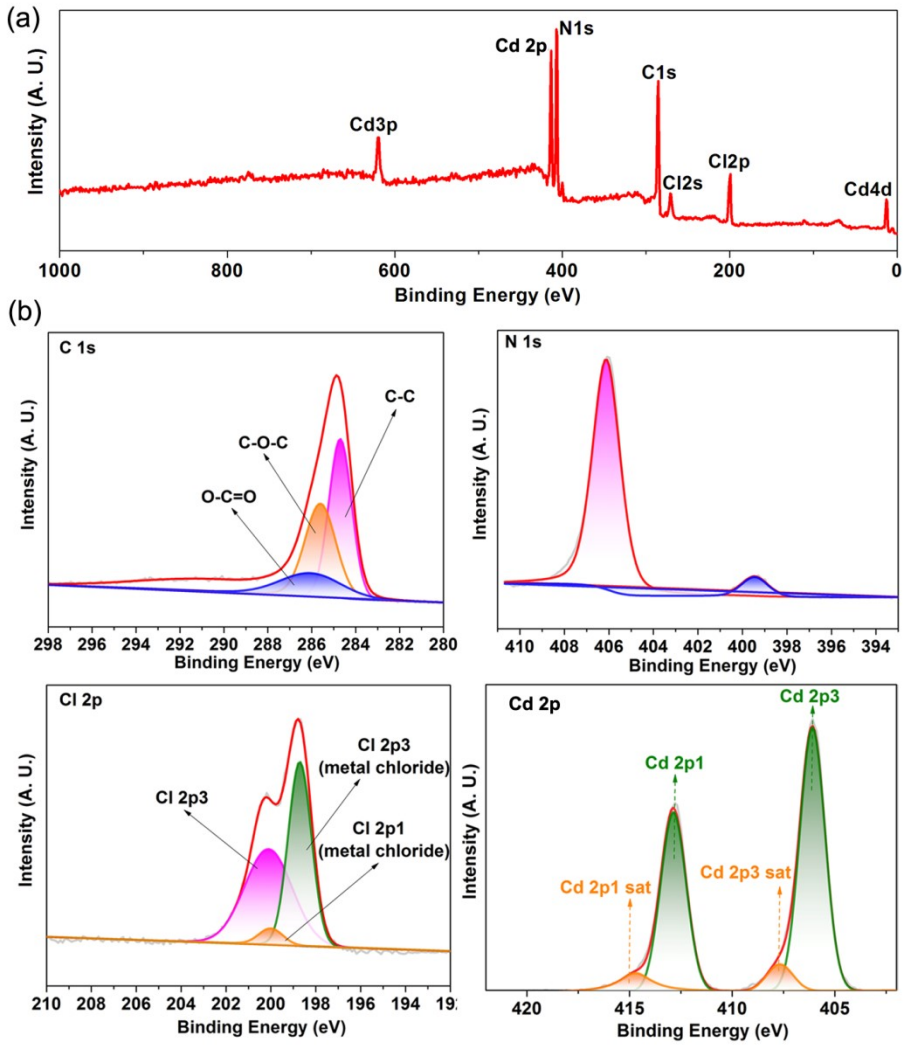

Figure S21. XPS spectrum (a), high-resolution XPS spectra of C 1s, N 1s, Cl 2p and Cd 2p (b) in **1** after photocatalytic degradation of MO.

3. Supporting Table

Table S1. Crystallographic data for **1.**

Complex	**1**
Chemical formula	$C_{13}H_9CdCl_2N$
Formula weight	362.51
Crystal system	Monoclinic
Space group	$P2_1/c$
a (Å)	17.095(2)
b (Å)	10.0218(10)
c (Å)	7.0974(8)
α (°)	90.00
β (°)	97.333(10)
γ (°)	90.00
V (Å^3)	1199.8(2)
Z	4
D (g cm^{-3})	2.007
μ (mm^{-1})	2.237
R_{int}	0.0631
Goof	1.391
$R_1{}^a$ ($I>2\sigma$ (I))^b	0.0994
$wR_2{}^a$ ($I>2\sigma$(I))^b	0.2296

[a] $R_1 = \Sigma(||F_o| - |F_c||)/\Sigma|F_o|$; [b] $wR_2 = [\Sigma w(|F_o|^2 - |F_c|^2)^2/\Sigma w(F_o{}^2)^2]^{1/2}$

Table 2. Selected bond lengths (Å) and angles (deg) for **1**[a].

Cd1–Cl1	2.496(3)	Cd1–Cl1^{A}	2.700(3)
Cd1–Cl2	2.495(3)	Cd1–Cl22	2.705(3)
Cl1–Cd1–Cl1^{A}	92.58(10)	Cl1–Cd1–Cl2^{B}	84.70(10)
Cl1^{A}–Cd1–Cl2^{B}	176.92(9)	Cl2–Cd1–Cl	111.51(11)
Cl2–Cd1–Cl1^{A}	84.84(10)	Cl2–Cd1–Cl2^{B}	94.80(11)
N1–Cd1–Cl1	124.25(19)	N1–Cd1–Cl1^{A}	91.60(19)
N1–Cd1–Cl2^{B}	91.13(18)	N1–Cd1–Cl2	124.23(18)

[a] Symmetry transformations used to generate equivalent atoms in **1**: A +*x*, 3/2-*y*, -1/2+*z*; B +*x*, 3/2-*y*, 1/2+*z*.

Table S3. Comparison of photophysical properties of some developed phosphors.

Phosphors	Maintain emission intensity at 423 K	Synthesis conditions	Emission peak (nm)	FWHM (nm)	PLQY (%)	Ref.
$[CdCl_2(AD)]$	84%	Solvothermal at 120°C for 3 h	504	100	65	This work
$LSN:Ce^{3+}$	55%	20MPa 600 °C for 30 min	550	–	–	7
$SCASN:Eu^{2+}$	59%	Sintered at 1800 °C for 2 h	640	–	–	7
$(Lu_{0.9}Ce_{0.1})_3Al_5O_{13}$	97%	Sintered at 1700 °C for 10 h	530	~120	–	7
$Na_3Sc_2(PO_4)_3:Eu^{2+}$	100%	Sintered at 1050 °C for 5 h	453	44	–	8
$[(AD)Pb_2Cl_5]$	47%	Hydrothermal at 120°C for 12 h	533	86	7.45	9
Tb-MOF	94.5%	Solvothermal at 130°C for 7 days	547	–	53	10
$K_3LuSi_2O_7:Eu^{2+}$	59%	Sintered at 1350 °C for 6 h	740	160	15	11
$ScBO_3:Cr^{3+}$	50%	Sintered at 1000 °C for 10 h	800	120	73	12
$SrAl_6Ga_6O_{19}:Cr^{3+}$	100%	Sintered at 1250 °C for 5 h	~770	~100	85	13
$YMAS:Cr^{3+}$	94%	Sintered at 1400 °C for 4 h	708	72	86	14
$CaMgSi_2O_6:Cr^{3+}$	88%	Sintered at 1250 °C for 4 h	780	~150	–	15
$NaLaMgWO_6$	72%	Sintered at 1300 °C for 9 h	698	~60	64.8	16

4. Supporting References

1 CrysAlisPro, Rigaku Oxford Diffraction, Version 1.171.39.6a.

2 G. M. Sheldrick, *Acta Crystallogr. Sect. A*. 2008, **A64**, 112–122.

3 G. M. Sheldrick, *Acta Cryst*. 2015, **A71**, 3–8.

4 B. Delley, *J. Chem. Phys*., 2000, **113**, 7756–7764.

5 S. J. Clark, M. D. Segall, C. J. Pickard, P. J. Hasnip, M. J. Probert, K. Refson, M. C. Payne, *Zeitschrift füer Kristallographie*, 2005, **220**, 567–570.

6 B. Delley, *J. Chem. Phys*., 1990, **92**, 508–517.

7 L. Chen, C.-C. Lin, C.-W. Yeh, R.-S. Liu, *Materials*, 2010, **3**, 2172–2195.

8 Y. H. Kim, P. Arunkumar, B. Y. Kim, S. Unithrattil, E. Kim, S.-H. Moon, J. Y. Hyun, K. H. Kim, D. Lee, J.-S. Lee, W. B. Im, *Nat. Mater*., 2017, **16**, 543–550.

9 X. G. Yang, L. F. Ma, D. Yan, *Chem. Sci*., 2019, **10**, 4567–4572.

10 Z. X. Lu, S. J. Wang, G.-L. Li, Z. Zhuo, H. M. Zhu, W. Wang, Y.-G. Huang, M. C. Hong, *ACS Appl. Mater. Interfaces,* 2022, **33**, 37894–37903.

11 J. W. Qiao, G. J. Zhou, Y. Y. Zhou, Q. Y. Zhang, Z. G. Xia, *Nat. Commun.,* 2019, **10**, 5267.

12 M.-H. Fang, P.-Y. Huang, Z. Bao, N. Majewska, T. Lesniewski, S. Mahlik, M. Grinberg, G. Leniec, S. M. Kaczmarek, C. W. Yang, K.-M. Lu, H.-S. Sheu, R.-S. Liu, *Chem. Mater.,* 2020, **32**, 2166–2171.

13 V. Rajendran, M.-H. Fang, W.-T. Huang, N. Majewska, T. Lesniewski, S. Mahlik, G. Leniec, S. M. Kaczmarek, W. K. Pang, V. K. Peterson, K. M. Lu, H. Chang, R. S. Liu, *J. Am. Chem. Soc.*, 2021, **143**, 19058–19066.

14 J. J. Feng, H. M. Liu, Z. Ma, J. H. Feng, L. F. Chen, J. H. Li, Q. G. Zeng, D. W. Wen, Y. Guo, *Chem. Eng. J.*, 2022, **449**, 137892.

15 D. W. Wen, H. M. Liu, Y. Guo, Q. G. Zeng, M. M. Wu, R. S. Liu, *Angew. Chem. Int. Ed*., 2022, **61**, e202204411.

16 S. Wu, P. X. Xiong, Q. Liu, Y. Xiao, Y. S. Sun, E. H. Song, Y. Chen, *Adv. Optical Mater.,* 2022, **23**, 2201718.